distribution of the model is seldom a good first-order approximation.

2) The pressure distribution on a steep afterbody exhibits a plateau pressure region near freestream pressure when the recirculation region is of considerable extent and depth.

3) The length of the separation region seems to be a function of Mach number, with larger regions and earlier separation occurring at high Mach numbers.

4) The point of separation on an afterbody cannot accurately be determined from the pressure distribution alone.

5) Large discrepancies exist between existing separation criteria and the data.

6) The separated region can be modeled fairly well by a conical dividing streamline surface between the point of separation and the point of reattachment. The inviscid pressure distribution over the body including this dividing streamline seems to be a good first-order approximation to the actual separated pressure field.

References

[1]Chang, R. K., *Separation of Flow*, Pergamon Press, New York, 1970, pp. 1-200.

[2]Kuehn, D. M., "Experimental Investigation of the Pressure Rise Required for the Incipient Separation of Turbulent Boundary Layers in Two-Dimensional Supersonic Flow," Memo 1-21-59A, 1959, NASA.

[3]Presz, W. M., Jr., "Turbulent Boundary Layer Separation on Axisymmetric Afterbodies," Ph.D. thesis, 1974, School of Engineering, Univ. of Connecticut, Storrs, Conn.

[4]Hahn, M., Rubbert, P., and Mahal, A., "Evaluation of Separation Criteria and Their Application to Separated Flow Analyses," AFFDL-TR-72-145, 1973, Air Force Flight Dynamics Lab., Wright-Patterson Air Force Base, Ohio.

[5]Stanewsky, E. and Little, B. H., "Separation and Reattachment in Transonic Airflow," *Journal of Aircraft*, Vol. 8, No. 12, Dec. 1971, pp. 952-960.

[6]Cebeci, T., Mosinski, G. J., and Smith, A. M. O., "Calculation of Separation Points in Incompressible Turbulent Flows," *Journal of Aircraft*, Vol. 9, No. 9, Sept. 1972, pp. 618-624.

[7]Reshotko, E. and Tucker, M., "Approximate Calculation of the Compressible Turbulent Boundary Layer with Heat Transfer and Arbitrary Pressure Gradient," TN-4154, 1957, NASA.

[8]Elliot, D. G., Bartz, D. R., and Silber, S., "Calculation of Turbulent Boundary Layer Growth and Heat Transfer in Axisymmetric Nozzles," TR-32-387, 1963, Jet Propulsion Lab., Pasedena, Calif.

[9]Stratford, B. S., "The Prediction of the Turbulent Boundary Layer," *Journal of Fluid Mechanics*, Vol. 5, 1959, pp. 1-16.

[10]Page, R. H., "A Theory for Incipient Separation," in *Developments in Mechanics*, Vol. 1, Plenum Press, New York, 1961, pp. 563-577.

[11]Eilers, R. E., "Analytical Investigation of Subsonic Separation from Axisymmetric Boattails," D6-20399, A68, 1968, Boeing Aircraft Co., Seattle, Wash.

[12]Goldschmied, F. R., "An Approach to Turbulent Incompressible Separation Under Adverse Pressure Gradients," *Journal of Aircraft*, Vol. 2, No. 2, March-April 1965, pp. 108-115.

[13]Mathews, D. C., Paynter, G. C., and Childs, M. E., "Use of Coles' Universal Wake Function for Compressible Turbulent Boundary Layers," *Journal of Aircraft*, Vol. 7, No. 2, March-April 1970, pp. 137-140.

[14]Smith, A. M. O. and Pierce, J., "Exact Solution of the Nuemann Problem; Calculation of Non-Circulatory Plane and Axial Symmetry Flow About or Within Arbitrary Boundaries," *Proceedings of the Third U.S. National Congress of Applied Mechanics*, Vol. 2, 1968, Brown University, Providence, R.I., pp. 807-815.

[15]Shapiro, A. H., *The Dynamics and Thermodynamics of Compressible Fluid Flow*, Vol. 1, Ronald Press, New York, 1953, pp. 303-426

Airfoil Design for High Tip Speed Compressors

G. David Huffman*
Indianapolis Center for Advanced Research and Indiana-Purdue University at Indianapolis, Ind.
and
P. C. Tramm†
Detroit Diesel Allison Division of General Motors, Indianapolis, Ind.

An investigation into the use of new airfoil designs to improve the efficiency of high tip speed fans and multistage compressors is in process. Two-dimensional cascade test data are presented for a conventional multiple circular arc airfoil design and for one designed to an unstarted strong oblique shock wave pattern. Both airfoils have a 1.588 design point inlet Mach number. Design flow conditions are generally achieved; the multiple circular arc airfoil has better performance at low pressure ratios and the airfoil using an unstarted strong oblique shock system is superior at high pressure ratios. A categorization of the losses is presented.

Presented as Paper 73-1248 at the AIAA/SAE 9th Propulsion Conference, Las Vegas, Nev., November 5-7, 1973; submitted February 21, 1974; revision received August 16, 1974. This work was carried out as one phase of the U.S. Air Force Turbine Engine/High Flow Compressor Program.[1]

Index categories: Airbreathing Propulsion, Subsonic and Supersonic; Subsonic and Transonic Flow.

*Center Fellow and Professor of Engineering and Adjunct Professor of Mathematical Sciences; formerly Chief, Mechanics Research, Detroit Diesel Allison. Associate Fellow AIAA.

†Chief, Internal, Aerodynamics Research. Member AIAA.

Nomenclature

A = area, in.^{2} (m^2)
c = airfoil chord, in. (mm)
C_p = static pressure coefficient, $[2(p - p_1)]/[k\, p_1\, M_1^2]$
D = diffusion factor, $1 - V_2/V_1 + \sin(\beta_2)[1 - V_{y2}/V_{y1}]/2\sigma$
k = ratio of specific heats
l = distance along the chord line from the leading edge, in. (mm)
M = Mach number
p = static pressure, lb$_f$/in.^{2} (pa)
P = total pressure, lb$_f$/in.^{2} (pa)
r = radius, in. (mm)

s = airfoil spacing, in. (mm)
t = airfoil thickness, in. (mm)
V = velocity, fps (m/sec)
β = angle measured from the axial direction, degrees (rad)
σ = solidity, c/sec
ω = total pressure loss coefficient, $(P_1 - P_2)/(P_1 - p_{1e})$
Ω = total pressure loss parameter, $\omega \cos(\beta_2)/2\sigma$

Superscripts
* = choked or airfoil mean line value

Subscripts
bw = bow wave
e = entrance
in = inflection
le = mean leading edge condition
max = maximum
min = minimum
p = profile
s = shock
te = trailing edge
tm = maximum thickness
y = tangential
1 = cascade inlet
2 = fully mixed and/or cascade exit condition

Introduction

FAN and compressor technology for air breathing propulsion systems is being advanced by operating these components at higher through flow velocities and higher rotational speeds. Increased through flow velocity results in a higher airflow rate and higher thrust for a given component size. The desired pressure ratio may be achieved with fewer fan and compressor stages as the rotational speed is increased. Greater through flow velocities and rotational speeds cause higher Mach numbers and often result in poorer component efficiencies associated with increased airfoil drag. Identifying these sources of increased drag and devising means for minimizing their magnitude is, therefore, a key to the process of advancing fan and compressor technology.

The usual compressor design practice dictates that the inlet Mach number relative to the rotor airfoils is higher than that for stator airfoils. For example, a rotor airfoil having a 1600 fps (488 m/sec) tip speed generally has a tip inlet relative Mach number of about 1.6 while an airfoil in the following stator row has a subsonic inlet absolute Mach number at all radial locations. Achieving satisfactory advanced fan and compressor efficiency is, therefore, chiefly concerned with the higher Mach number rotor airfoils.

Rotor airfoil surface pressures and wakes may be easily measured during stationary two-dimensional cascade testing. The same rotor airfoil measurements are obtained within a compressor only with extreme difficulty. A number of authors[2,3] have shown that the flow processes within a two-dimensional cascade tunnel are a reasonably good facsimile of that within a compressor. The two-dimensional cascade tunnel can, therefore, be utilized in the evaluation of high Mach number rotor airfoils.

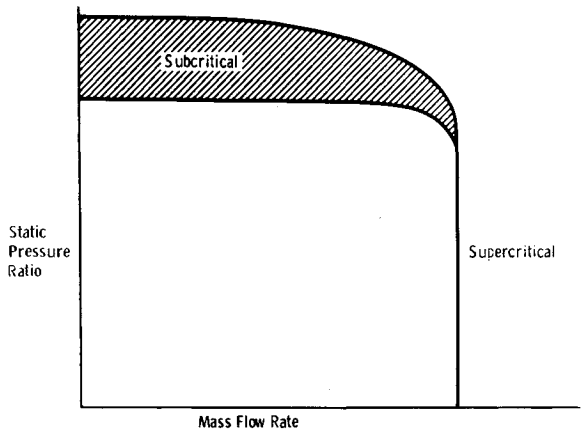

Fig. 1 Cascade operating modes.

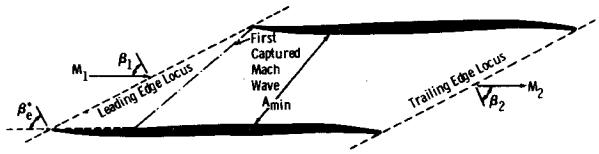

Fig. 2 Airfoil cascade parameters.

This paper presents the results of two-dimensional supersonic cascade tunnel tests of two rotor airfoil sections designed for the same inlet conditions. General aerodynamic considerations as well as specific details of the two rotor airfoil sections are given. Facilities and test procedures are discussed. Test results are analyzed to determine the sources of drag.

Aerodynamic Design Considerations

Inlet conditions for the two rotor airfoil cascades consist of a relative Mach number of 1.588 with an axial component of 0.778, i.e., the airfoils are of the subsonic leading edge locus type. The operation of this type of cascade resembles that of a supersonic airbreathing engine inlet. Both have two operating ranges, i.e., supercritical and subcritical as shown in Fig. 1. During supercritical operation, a region of supersonic flow extends across the passage formed by adjacent airfoils such that variations in downstream operating conditions cannot be felt upstream of the cascade. On the other hand, subcritical operation is characterized by a predominantly subsonic passage flow which permits downstream to upstream communication.

Nomenclature for upstream and downstream conditions as well as several airfoil parameters is shown in Fig. 2. A_{min} denotes the area of the passage formed by adjacent airfoils at the throat, i.e., the minimum value. A left running Mach wave interests the suction surface and the leading edge of the adjacent airfoil as shown in Figs. 2 and 3. The portion of the suction surface upstream of this point is referred to as the entrance region, e.g., see Fig. 3, and is the only element of the airfoil influencing the upstream flow during supercritical operation. β^*_e is defined as the angle between the secant line drawn through the afore-mentioned point and the leading edge and the axial direction. This is also known as the setting angle of the entrance region.

The operating modes for cascades of the subsonic leading edge locus variety are primarily determined by the area ratio, A_{min}/A^*, and the incidence, $\beta_1 - \beta^*_e$. A^* denotes the critical throat area as determined by the Kantrowitz starting criterion.[4] An area ratio greater than one implies some margin for achieving a started passage condition. The interactions between the incidence, area ratio, and the cascade operating regimes are shown in Fig. 4. Ideally the cascade cannot operate at negative values of entrance region incidence nor values of area ratio less than one.

Figure 4 is dominated by two constraint conditions, i.e., $\beta_1 - \beta^*_e = 0$ and $A_{min}/A^* = 1$. At any point on these

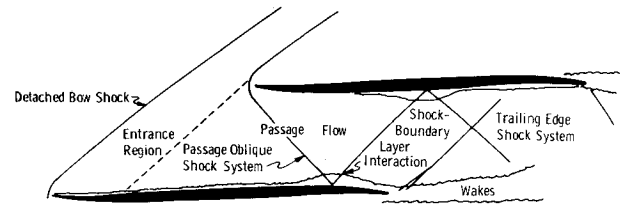

Fig. 3 Flow regions within an airfoil cascade of the subsonic leading edge locus type.

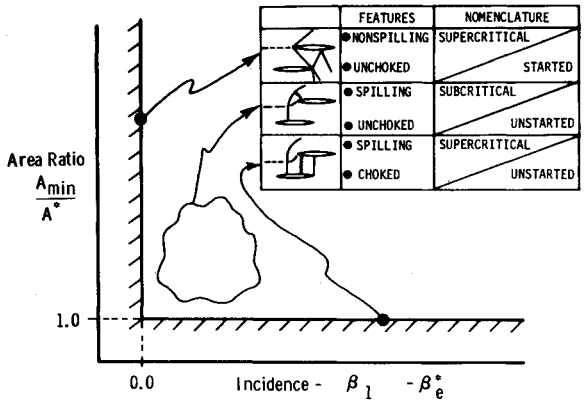

Fig. 4 Cascade operating regimes.

lines the operation is supercritical. They differ in that one is started, $\beta_1 = \beta^*_e$, and the other is unstarted, $A_{\min} = A^*$. When both $\beta_1 > \beta^*_e$ and $A_{\min} > A^*$, the cascade operates in the subcritical mode. If $\beta_1 > \beta^*_e$, the bow wave of Fig. 3 is detached from the leading edge and flow spills reducing the passage mass flow rate.

The values of the constraint conditions are effected by additional aerodynamic considerations. In particular, the entrance region incidence is influenced by the leading edge radius and the entrance region boundary layer development. In actual practice, the incidence condition is given approximately by

$$\beta_1 - \beta^*_e \geq 1.5^\circ (0.026 \text{ rad}) \quad (1)$$

The minimum area ratio is effected by passage and/or airfoil camber and boundary layer blockage at the throat. As a result, the area ratio constraint is increased approximately to 1.03 in the 1.5 Mach number range, i.e.,

$$A_{\min}/A^* \geq 1.03. \quad (2)$$

As the inlet Mach number increases, the area ratio may become appreciably less than one.[5] This is the result of a strong interaction between the passage oblique shock system and the suction surface boundary layer causing separation and a departure from the nearly normal shock used in the definition of the $A_{\min}/A^*$ constraint.

The previous discussion of the operating characteristics of a supersonic cascade with subsonic leading edge locus provides groundwork for a more detailed exposition of specific aerodynamic design considerations.

Leading Edge and Entrance Region

The performance of the cascade may be influenced in several ways by the airfoil leading edge. As previously stated, the leading edge thickness and/or radius is important in determining the started flow incidence, i.e., as r_{le}/c is increased, $\beta_1 - \beta^*_e$ must be increased for started flow. Figure 3 indicates that the entrance region contains only left running waves and, thus, an increase in incidence results in increasing the entrance region suction surface Mach number. This contradicts the overall objective of the cascade and must be minimized.

Airfoil structural considerations dictate that the leading edge radius assumes a finite value. As a consequence, a detached bow wave is formed as shown in Fig. 3 and a corresponding total pressure loss results. This loss is approximately proportional to the leading edge thickness.[6,7] The bow wave total pressure loss is strongly Mach number dependent—increasing with increased inlet Mach number.

The distribution of bow wave total pressure loss effects the suction and pressure surface boundary layer development. Streamlines at the edge of the boundary layer have lower stagnation pressure than those in the freestream. This promotes boundary-layer growth and improves chances for separation.

Most supersonic airfoil leading edges are round. The flow in the vicinity of the leading edge will, thus, resemble flow around a right circular cylinder. Wind tunnel tests[8] of this configuration indicate that a substantial pressure deficit is developed at a point on the surface which is tangent to the freestream direction. Shortly downstream of this point, the flow will be compressed back to its freestream value causing thickening of the suction surface boundary layer. This effect can also be reduced by decreasing the leading edge radius.

Aside from the leading edge, the entrance region is the only portion of the airfoil which influences the upstream flow during started operation. For two-dimensional cascade airfoils, upstream influences are minimized when the entrance region is a straight-line segment which suggests that this type of entrance region is near optimum.

Throat Area

In a manner analogous to a supersonic inlet for an air-breathing engine, various combinations of internal and external contraction may be selected to accomplish the desired overall pressure ratio. The degree of contraction is limited by the value of throat area required to satisfy the starting area ratio constraint as previously discussed. External contraction, i.e., located downstream of the entrance region and forward of the passage entrance, causes a reduction in passage entrance Mach number and results in a smaller allowable throat area. If only modest diffusion is required, the optimum throat area may be somewhat larger than the value determined by the starting area ratio constraint. Furthermore, performance at Mach numbers which are less than the design value may be improved by using a throat area which exceeds the optimum design point value.

Exit Region

The exit region is defined as the portion of the airfoil's pressure surface which is downstream of the passage formed by adjacent airfoils, e.g., see Fig. 3. The exit region is similar to the entrance region in that it influences the downstream flow in a manner analogous to the entrance region's effect on the upstream flow. The exit Mach numbers typically range from 0.9 to 1.4 for pressure ratios varying from 1.2 to 2.2. The near sonic downstream flow is least disturbed when the exit region consists of a straight line segment. Substantial curvature will likely result in the formation of shock waves and separation from this portion of the pressure surface. Even under optimum conditions, the flow leaving the cascade may be relatively nonuniform as a consequence of a shock system which has its origins at the trailing edge or in the passage formed by adjacent airfoils. In some cases, this wave system has been a source of considerable total pressure loss.

Shock Wave Boundary-Layer Interactions

It would be desirable to construct the airfoil such that the surface pressure distributions were characterized by continuous compression, i.e., no shock waves impinged on the airfoil. This type of design would minimize the possibility of boundary-layer separation. In practice, this is difficult to achieve and either expansion zones or shock wave-boundary-layer interactions are accepted.

Airfoil Designs

The previous sections establish the bulk of the reasoning utilized in the design of the two airfoil sections. A description of the designs is presented in the ensuing sec-

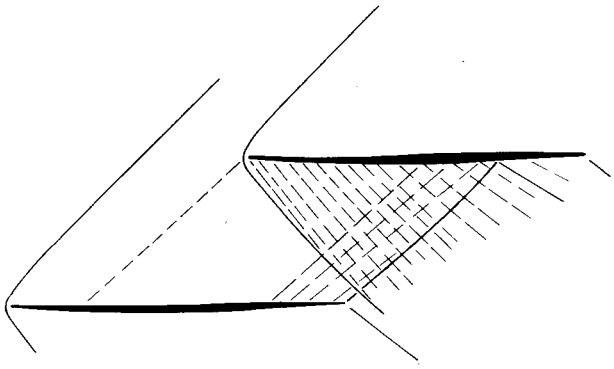

Fig. 5 MCA airfoil and the design wave pattern. $M_1 = 1.588$.

tions. Both airfoil sections have the same chord, 2.5 in. (635 mm) and leading edge radius, 0.005 in. (127 μm). The first airfoil is a multiple circular arc (MCA) configuration which represents conventional design practice.[9] Its performance is used as a standard of comparison for the alternate design. The remaining airfoil is intended for operation in the unstarted mode, i.e., an unstarted strong oblique shock (USO) airfoil.

Multiple Circular Arc Airfoil

This configuration has a meanline consisting of two circular arcs and a parabolic thickness distribution. The circular arcs are joined at an inflection point where they have the same slopes. The thickness is measured normal to the meanline and is determined from two functions of meanline arc length. One function applies from the leading edge to the maximum thickness location and the other applies for the remainder of the meanline. The nine parameters determining the design are: maximum thickness to chord ratio, leading edge radius to chord ratio, trailing edge radius to chord ratio, spacing to chord ratio, the location of maximum thickness, the inflection point location, and the meanline leading edge, inflection point, and trailing edge angles. Values of the afore-mentioned parameters as well as the relevant aerodynamic conditions are given in Table 1. The conventional loss model[10] was used to predict the total pressure loss coefficient, ω.

Values of the first five parameters of Table 1 are typical of conventional MCA fan rotor tip airfoil sections. The sixth parameter, l_{in}/c, has been chosen so that the inflection point occurs at the passage entrance. The quantity, $\sigma \sin \beta^*_1$ is used to determine l_{in}/c. Values for the three meanline angles are determined by specifying three design constraints: an entrance region incidence of 1.5° (0.026 rad), a A_{min}/A^* ratio of 1.03, and a zero deviation angle between the trailing edge pressure surface tangent and the exit flow direction.

This group of parameters should result in started mode operation at the design point. The MCA airfoil design and its wave pattern—predicted by the method of characteristics—is shown in Fig. 5. The airfoil has negative camber in its forward portion resulting in an approximately straight line entrance region segment and a corresponding expansion system on the forward portion of the pressure surface. A strong interaction takes place between the left running trailing edge compression wave and the pressure surface boundary layer of the adjacent airfoil. A system of shock waves exists in the downstream flowfield for this operating point.

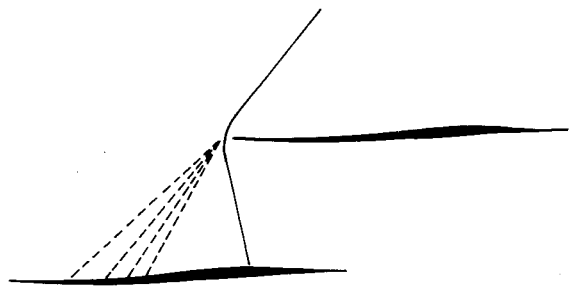

Fig. 6 USO airfoil and the design wave pattern. $M_1 = 1.588$.

Table 1 Airfoil design parameters

Parameter	MCA	USO
t_{max}/c	0.025	0.025
r_{le}/c	0.002	0.002
r_{te}/c	0.002	0.002
σ	1.217	1.289
l_{tm}/c	0.500	0.700
l_{in}/c	0.713	...
β_1	60.32° (1.053 rad)	59.50° (1.038 rad)
β^*_1	56.66° (0.989 rad)	57.11° (0.997 rad)
β_2	61.40° (1.072 rad)	65.19° (1.138 rad)
β^*_2	57.74° (1.008 rad)	62.98° (1.099 rad)
β^*_{in}	60.78° (1.061 rad)	...
M_1	1.588	1.588
M_2	0.982	1.000
ω	0.241	0.121

Unstarted Strong Oblique Shock Airfoil

As previously stated, this airfoil is designed to operate in the unstarted mode. A combination of two-dimensional boundary layer and potential flow techniques was used to establish the desired pressure distribution and corresponding airfoil shape. The intended wave pattern and airfoil shape are shown in Fig. 6. The design intent employed in this instance is qualitatively similar to that used by Morris et al.[11]

The entrance region is again a straight line segment with a leading edge wedge angle of 3° (0.052 rad). Compression is achieved by a left running wave system emanating from the convex portion of the suction surface just aft of the entrance region and by a right running strong oblique shock wave which is a continuation of the leading edge bow wave. The Mach number downstream of this shock is approximately 0.9. A straight line segment—parallel with the desired exit flow direction—is used for the exit region. The passage formed by adjacent airfoils consists of arcs from two concentric circles. Radii of the pressure and suction surface arcs equal six and seven passage heights, respectively. Displacement thicknesses are obtained from boundary-layer calculations and are used to determine the actual airfoil surface once the effective surface has been established. An exception is in the region of the strong oblique shock interaction with the suction surface boundary layer. Calculations indicate separation in this region and experimental results[12] for a similar situation are used to establish the displacement thickness. Reattachment should occur immediately upstream of the trailing edge.

Of the two designs, the USO configurations has the highest solidity. Moreover, the A_{min}/A^* ratio for the USO design is 0.99 and the predicted total pressure loss coefficient is 0.121 based on the design wave system and boundary layer thicknesses. Airfoil parameters are included in Table 1.

Experimental Facilities

The airfoil cascades were designed for operation in the supersonic wind tunnel shown in Fig. 7. This tunnel uses filtered, dried, and temperature controlled air and is a

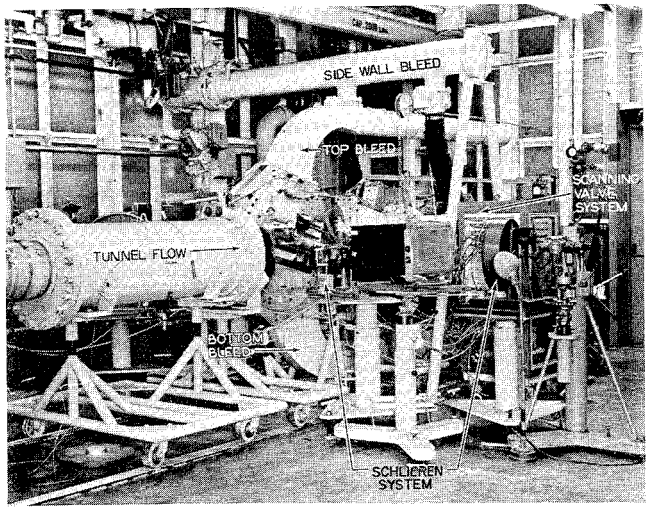

Fig. 7 Over-all view of the supersonic wind tunnel.

continuous flow, nonreturn system. The test section exit is evacuated by steam ejectors. The nozzle block boundary layers are removed by means of upper and lower bleed ducts (see Fig. 8). An auxiliary steam ejector is used to remove the sidewall boundary layers. The test section is mechanized so that a cascade of airfoils can be rotated while the tunnel is operating.

Cascade Experimental Design

A number of general factors must be considered in the design of a cascade experiment. First, the proper inlet flow conditions must be established. Second, the exit conditions must be set up correctly for they are no less important or less difficult to simulate than the inlet flow conditions. Third, the blade aspect ratio must be chosen such that all experimental data is obtained at the same value of the axial velocity-density ratio.

With respect to the cascade inlet conditions, consideration must be given to flow velocity, flow direction, and the institution of a periodic flow pattern to simulate an infinite cascade. The following features are incorporated in the cascade design in order to provide the desired flow conditions:

1) *Top and bottom bleed system.* The bleed system prevents the nozzle boundary layers from entering the cascade flowfield. They also provide paths for spillage so that the exit and inlet operate independently.

2) *Upstream wedge.* A sharp wedge is mounted upstream of the cascade. The inlet flow direction and Mach number are determined by the orientation of the wedge with regard to the airfoils and the nozzle flow, respectively.

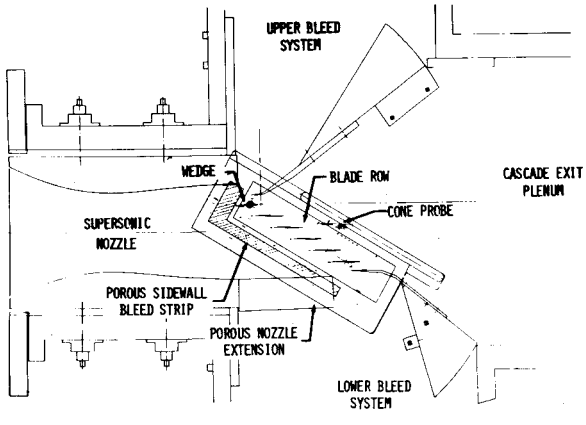

Fig. 8 Compressor cascade test section schematic.

In order to obtain the desired two-dimensional cascade configuration, i.e., an axial velocity-density ratio of one, and minimize sidewall boundary-layer-cascade flow interactions, a boundary-layer control system is employed. The system utilizes a porous bleed strip and is shown in Fig. 8. This type device is not optically restrictive and schlieren photographs of the cascade were obtained.

Data Acquisition and Processing

The wind tunnel of Fig. 7 is equipped with an instrumentation system which is centered around a laboratory-sized digital computer providing rapid on-line data acquisition and reduction. The use of the computer makes it possible to acquire raw data, convert it to engineering units, and make computations while the experiment is in progress. This enables personnel to evaluate the experimental data during the test. Decisions to repeat some phases of the test can be made instantly.

The digital computer is used for control of instrumentation, data acquisition, and data reduction. In this mode, the computer operates a digital voltmeter, an electronic scanner, stepping motors used in pressure measurements, indexer for positioning the conical probe, and the computer input/output equipment. During wind-tunnel operation, the computer automatically acquires all data required to determine the cascade performance characteristics. Pressure measurements are obtained from four 48 port computer controlled rotary valves providing a pressure measurement capacity of 192 channels. Differential pressure measurements are obtained from individual transducers as required. The test section angular setting and the cone probe position are also measured using the computer system.

During data acquisition, the computer performs two additional functions. The first three active ports on each of the four rotary valves are used for three reference calibration pressures. Each time the computer initiates a set of pressure readings, the reference values are measured providing direct on-line calibration of the pressure transducers. Secondly, the wind-tunnel total pressure and temperature are monitored during each test point. If the temperature or pressure varies outside a preset tolerance, the computer automatically presents the out-of-limit reading. The immediate data can be rejected and remeasured, the complete data set for the test point rejected and a new data set initiated, or the out-of-limits condition can be overridden and the test continued.

After the desired test condition is established, the on-line instrumentation system completes the acquisition and reduction of the experimental data. This includes defining the cascade inlet flowfield, positioning a conical probe at discrete points downstream of the airfoils to determine blade-to-blade flowfield properties, mass averaging and mixing[13] the blade-to-blade data thus specifying equivalent uniform properties, defining airfoil surface and sidewall performance, and plotting airfoil and blade-to-blade distributions of selected flowfield properties. For each test condition, a total of 450 measurements were made to define the cascade performance. The data reduction procedures are described in detail by McClure et al.[14]

Analysis of Results

The experimental results are subdivided into three areas and discussed in the following sections. First, the cascade operating regimes are reviewed. Second, the measured and predicted airfoil pressure distributions are discussed. Third, the over-all cascade performance is reviewed and the total pressure loss coefficient is broken down into its major elements.

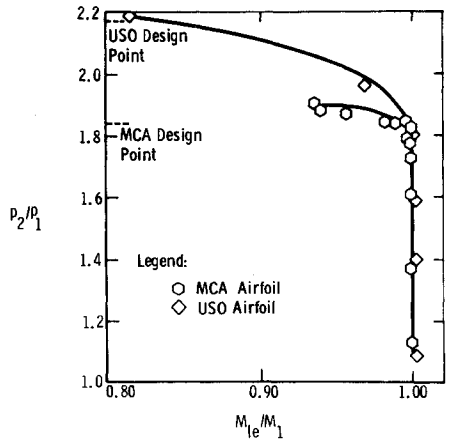

Fig. 9 Experimentally determined cascade operating modes. $M_1 = 1.588$.

Cascade Operating Modes

Regions of subcritical and supercritical operation were determined by means of sidewall static pressure taps just forward of the airfoil leading edge. These measurements are very sensitive to changes in bow wave position and can be used to indicate subcritical operation. The leading edge Mach number is computed by averaging the leading edge static pressure measurements and

$$M_{le} = \left\{ \frac{2}{k-1} \left[\left(\frac{P_1}{p_{le}} \right)^{\frac{k-1}{k}} - 1 \right] \right\}^{1/2} \quad (3)$$

A change in M_{le} while M_1 is constant implies a subcritical operating point. M_{le}/M_1 as a function of the static pressure ratio, p_2/p_1, for the two cascades is shown in Fig. 9. Figure 1 indicates that a vertical slope corresponds to supercritical operation while a non-vertical slope denotes a subcritical regime. It is quite obvious that both cascades exhibit an extensive supercritical and subcritical operating range with the transition between the two occurring abruptly. The MCA cascade achieves its design pressure ratio prior to spill or subcritical operation. The USO cascade operates subcritically at its design pressure ratio. The MCA and USO designs exhibit unsteady flow during subcritical operation; however, the flow is stable under supercritical conditions.

Figures 10 and 11 are schlieren photographs of the MCA cascade at static pressure ratios of 1.160 and 1.777. The leading edge pressure taps are clearly visible. Even though there is a substantial variation in static pressure ratio, the bow and passage oblique shock systems are similar indicating that the bulk of the compression process is occurring in the trailing edge shock system.

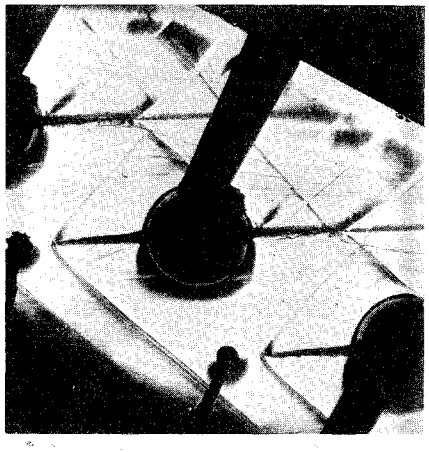

Fig. 10 Schlieren photograph of the MCA cascade. $M_1 = 1.588$ and $p_2/p_1 = 1.160$.

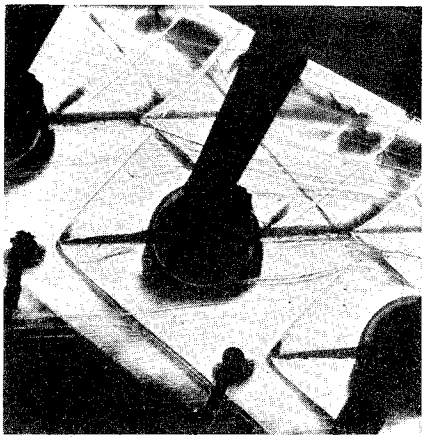

Fig. 11 Schlieren photograph of the MCA cascade. $M_1 = 1.588$ and $p_2/p_1 = 1.777$.

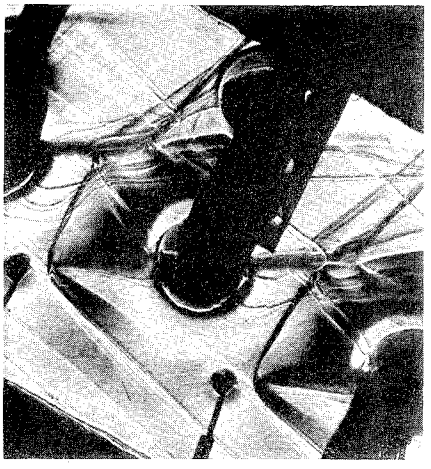

Fig. 12 Schlieren photograph of the USO cascade. $M_1 = 1.588$ and $p_2/p_1 = 1.087$.

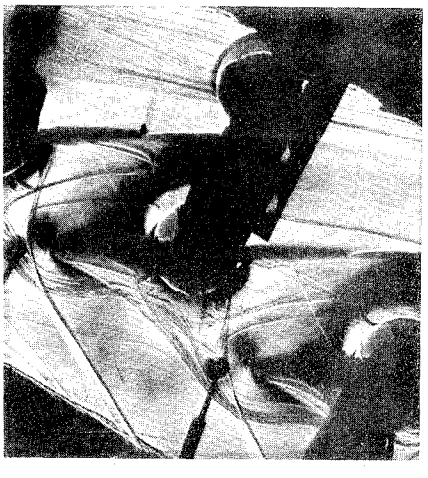

Fig. 13 Schlieren photograph of the USO cascade. $M_1 = 1.588$ and $p_2/p_1 = 2.195$.

Schlieren photographs of the USO cascade are shown in Figs. 12 and 13. In this case, a supercritical and subcritical operating point have been chosen. A substantial increase in the bow wave detachment distance occurs under subcritical conditions and manifests itself as a reduction

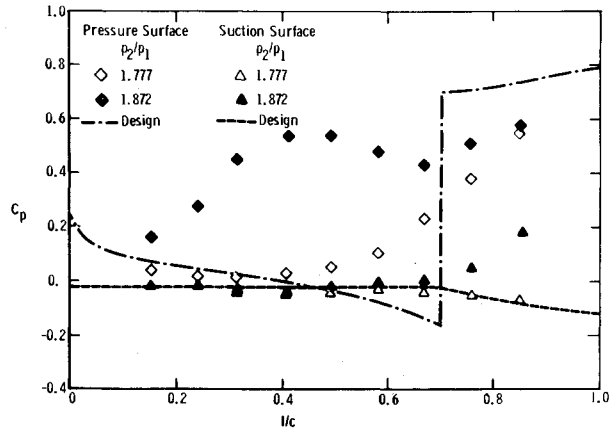

Fig. 14 Static pressure coefficient distribution for the MCA cascade. M_1 = 1.588.

in M_{le}/M_1. At a p_2/p_1 value of 2.195, the bulk of the pressure rise is accommodated by the nearly normal passage shock wave.

Airfoil Surface Pressure Coefficients

Airfoil static pressure distributions for an inlet Mach number of 1.588 are shown in Figs. 14 and 15 for the MCA and USO cascades, respectively. The static pressure distribution is presented as the variation of static pressure coefficient with chordwise location for both the suction and pressure surfaces. Design values of the static pressure distribution are compared to the experimental results at two static pressure ratios, i.e., the points having the highest supercritical and subcritical pressure ratios.

The MCA values of Fig. 14 for supercritical and subcritical operation at static pressure ratios of 1.777 and 1.872, respectively, differ considerably in shape which is consistent with the change in operating mode. The design values are in closer agreement with the supercritical case than with the subcritical one. The measured suction surface supercritical pressure distribution is virtually identical to the design predictions. The pressure surface values differ in the vicinity of the passage shock impingement point. The calculations treated the impinging shock as a zero thickness discontinuity while the pressure increase actually occurs over a finite distance. For the subcritical static pressure ratio, 1.872, the pressure surface shock impingement point has moved forward resulting in a possible boundary-layer separation. The suction surface pressure distributions are similar in both cases.

USO experimental values of static pressure coefficient are compared to design values in Fig. 15. The measured subcritical pressure distribution, i.e., p_2/p_1 = 2.195, is

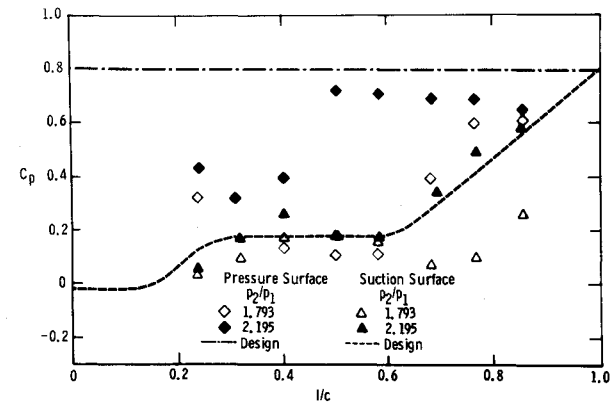

Fig. 15 Static pressure coefficient distribution for the USO cascade. M_1 = 1.588.

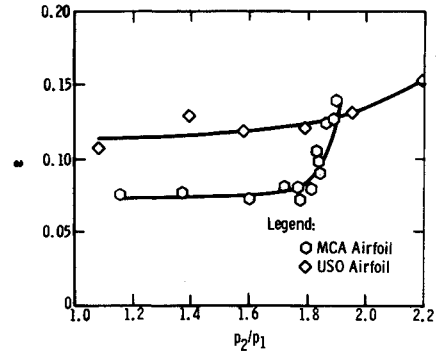

Fig. 16 Over-all cascade aerodynamic efficiency. M_1 = 1.588.

within ±0.1 of the design values except on the forward one-half of the pressure surface. The convex circular arc which forms this portion of the airfoil surface apparently causes a reduction in the static pressure coefficient which was neglected in the design predictions and may lead to an unanticipated thickening of the pressure surface boundary layer. The predicted shock impingement location, i.e., an l/c of 0.67, is in agreement with the measured value.

Over-All Cascade Performance

The aerodynamic efficiencies of the two designs are compared by considering the variation of total pressure loss coefficient, ω, with static pressure ratio. Fig. 16. All data are again for a design inlet Mach number of 1.588. The MCA cascade has the lowest total pressure loss coefficients at low to intermediate pressure ratios; however when p_2/p_1 values exceed 1.9, the USO design is superior. The USO cascade has total pressure loss coefficients values which are consistent with the design prediction of 0.121. On the other hand, the MCA airfoil losses are much less than the calculated value of 0.241 except at subcritical operating points.

The total pressure loss coefficient can be subdivided into shock and profile components by analyzing the blade-to-blade pressure measurements. In particular it is assumed that

$$\omega = \omega_s + \omega_p \tag{4}$$

where

$$\omega_s = \frac{P_1 - P_{2\max}}{P_1 - p_{le}} + \omega_{bw} \tag{5}$$

The bow wave loss coefficient is obtained theoretically and varies from 0.011 to 0.008 for the MCA cascade for the supercritical and subcritical conditions, respectively. The USO values range from 0.011 to 0.003 for the two operating modes. The profile total pressure loss coefficient

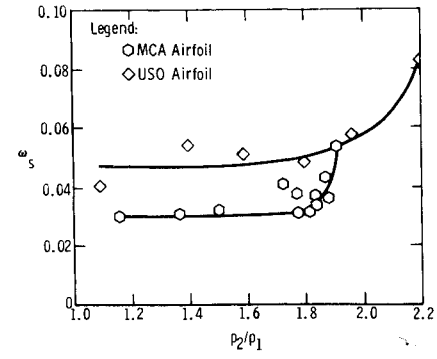

Fig. 17 Shock total pressure loss coefficient. M_1 = 1.588.

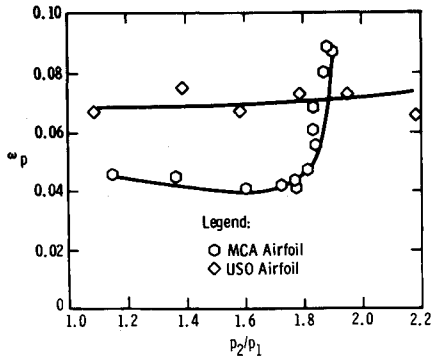

Fig. 18 Profile total pressure loss coefficient. $M_1 = 1.588$.

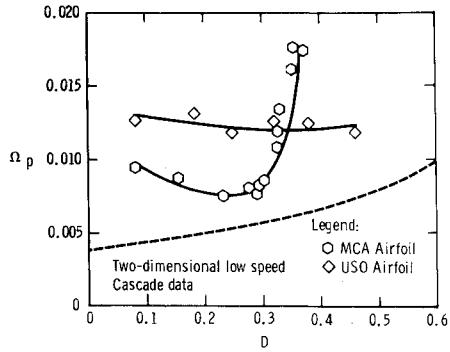

Fig. 19 Profile total pressure loss parameter. $M_1 = 1.588$.

can be further characterized by the profile loss parameter where

$$\Omega_p = \omega_p \cos \beta_2/2\sigma \quad (6)$$

The results of the aforementioned analysis are presented in Figs. 17–19. Again all values correspond to an inlet Mach number of 1.588. The shock total pressure losses vary from about 0.03 to 0.08 for supercritical and subcritical operation. These values range from about one-quarter to one-half of the Hartmann[10] value of 0.133 at a M_1 value of 1.588.

The profile total pressure losses are shown in Figure 18. As might be expected, the USO values are fairly uniform throughout the pressure ratio range. This is due to the dominance of the losses by the suction surface boundary-layer-shock wave interaction which is not strongly dependent on the pressure ratio; e.g., see Fig. 15. The MCA cascade values, however, vary markedly from the supercritical to the subcritical case. This may be due to the occurrence of a pressure surface boundary-layer separation at the higher static pressure ratios. The presence of separated regions on the airfoil surfaces contributes to the profile losses in an indirect manner. At the separation point, the skin friction approaches zero and, thus, the viscous drag decreases; however, the form drag generated by the separation bubble is proportional to the square of the velocity and increases drastically for high Mach numbers. Consequently, extensive regions of separated flow can markedly influence profile losses.

The profile total pressure loss parameter is shown in Fig. 19 and is similar to Fig. 18. The use of this grouping of variables has reduced the data scatter somewhat; nevertheless, the rapid increase in profile losses for the MCA cascade under subcritical conditions is still present. The dashed line in this figure—labeled Two-dimensional low speed Cascade data—is from a correlation[15] of NASA 65 series airfoil experiments at very low Mach numbers. The MCA cascade is approaching this limit even though there is a substantial increase in Mach number.

Conclusions

Based on the analysis of the experimental results for the airfoil cascades, the following conclusions can be drawn. 1) The MCA is superior to the USO cascade in the supercritical mode while the converse is true for subcritical operation. 2) The USO cascade achieves the highest static pressure ratio. 3) The experimental flow patterns generally agreed with the design intent. 4) The shock total pressure loss is usually less than half the value predicted by the Hartmann method. 5) Neither of the cascades represents an optimum design. Furthermore it is recommended that leading edge effects be investigated in detail and particular attention be given to the airfoil pressure surface.

References

[1]"Turbine Engine High Flow Compressor: Semi-Annual Technical Report Number 1," EDR 7674, Dec. 1972, Detroit Diesel Allison, Indianapolis, Ind.

[2]"Aerodynamic Demonstration and Design Analysis for High Tip Speed Fans and Compressors: Semi-Annual Technical Report," EDR 7317, Jan. 1972, Detroit Diesel Allison, Indianapolis, Ind.

[3]Mikolajczak, A. A. et al., "Comparison of Performance of Supersonic Blading in Cascade and in Compressor Rotors," *Journal of Engineering for Power*, Vol. 93, Jan. 1971, pp. 42–48.

[4]Kantrowitz, A. and Donaldson, C. DuP., "Preliminary Investigation of Supersonic Diffusers," ARR No. L5D20, 1945, NACA.

[5]Mitchell, G. A. and Cubbison, R. W., "An Experimental Investigation of the Restart Area Ratio of a Mach 3 Axisymmetric Mixed Compression Inlet," TMX-1547, April 1968, NASA.

[6]Klapproth, J. F., "Approximate Relative-Total-Pressure Losses of an Infinite Cascade of Supersonic Blades with Finite Leading Edge Thickness," RM E9L21, 1950, NACA.

[7]York, R. E. and Woodard, H. S., "Flow in the Entrance Region of Supersonic Compressor Cascades," EDR 8224, July 1974, Detroit Diesel Allison, Indianapolis, Ind.

[8]Gowen, F. E. and Perkins, E. W., "Drag of Circular Cylinders for a Wide Range of Reynolds Numbers and Mach Numbers," TN-2960, 1953, NACA.

[9]Monsarrat, N. T., et al. "Single Stage Evaluation of Highly-Loaded High-Mach-Number Compressor Stages," CR-72562, 1969, NASA.

[10]Miller, G. R. et al., "Shock Losses in Transonic Compressor Blade Rows," *Journal of Engineering for Power*, Vol. 83, July 1961, pp. 235–242.

[11]Morris, A. L. et al., "High-Loading, 1800 ft/sec Tip Speed Transonic Compressor Fan Stage: Phase I. Aerodynamic and Mechanical Design," CR-120907, 1972, NASA.

[12]Seddon, J. D., "The Flow Produced by Interaction of a Turbulent Boundary Layer with a Normal Shock of Strength Sufficient to Cause Separation," RAE TM 667, Royal Aircraft Establishment, Fornborough, England.

[13]Huffman, G. D., "An Analysis of Flow Mixing Following Airfoil Cascades," RN 71-78, Dec. 1971, Detroit Diesel Allison, Indianapolis, Ind.

[14]McClure, R. B. et al., "Investigation of a Supersonic Compressor Cascade with Contained Shock Blades," RN 71-60, Nov. 1971, Detroit Diesel Allison, Indianapolis, Ind.

[15]Johnson, I. A. and Bullock, R. O., "Aerodynamic Design of Axial-Flow Compressors, Revised," NASA SP-36, 1965, p. 205.